

Imaging the crustal structure beneath the Longmenshan fault zone and geodynamics for Wenchuan Mw 7.9 and Lushan Ms 7.0 earthquakes

Shengqing Xiong¹, Hai Yang¹, Qiankun Liu¹, Xue Yang¹, Zhaoliang Li¹, and Chong Fu²

¹China Aero Geophysical Survey and Remote Sensing Center for Natural Resources

²China University of Geosciences

November 24, 2022

Abstract

Although many velocity and electrical models have been proposed in the Longmenshan fault zone (LFZ) and its neighboring areas, the deep structure of seismic gap and the geodynamics of two different earthquakes remain uncertain. Based on aeromagnetic and gravity data, the Sichuan basin shows two NE-trending banded and strong positive magnetic anomalies and high Bouguer gravity anomalies. The banded magnetic anomalies represent the Neoproterozoic magmatic events in the center of Sichuan basin, rather than the rigid Neoproterozoic and Paleoproterozoic crystalline basement. The Songpan-Ganzi fold belt (SGFB) is weak positive magnetic and low Bouguer gravity anomalies. The LFZ is the boundary of two anomaly areas but similar to the feature of Sichuan basin. Three models are created by 2D magnetic and gravity forward modeling and provide more reliable and integrated geophysical interpretation for the deep structure of earthquake epicenter and seismic gap. The models reveal that the crust of Sichuan basin consists of double layer magnetic basement. More importantly, the basement subducted to about 33km west of the Wenchuan-Maoxian fault with low dip angle beneath the middle segment of the LFZ, whereas the distance decrease to about 17 and 19 km under the south segment. So, the crust of Sichuan basin beneath the middle segment extends further than the one beneath the south segment with the seismic gap as transition zone. Therefore, we propose the irregular shape of basement in western margin of Sichuan basin maybe the main reason for the different focal mechanism and geodynamic of Wenchuan and Lushan earthquakes.

1 **Imaging the crustal structure beneath the Longmenshan fault zone**
2 **and geodynamics for Wenchuan Mw 7.9 and Lushan Ms 7.0**
3 **earthquakes**

4
5 Shengqing Xiong ¹, Hai Yang ^{1,2}, Qiankun Liu ¹, Xue Yang ¹, Zhaoliang Li ¹, Cong
6 Fu³

7
8 ¹China Aero Geophysical Survey and Remote Sensing Center for Natural Resource,
9 Beijing, 100083

10 ²State Key Laboratory of Lithospheric Evolution, Institute of Geology and
11 Geophysics, Chinese Academy of Sciences, Beijing, 100029

12 ³China University of Geosciences, Beijing, 100083

13
14 Corresponding author: Hai Yang (yanghai@agr.cn)

15
16 **Keypoint:**

17 1. The crust of Sichuan basin beneath the middle segment of the LFZ extends further
18 than the one beneath the south segment.

19 2. The basement of Sichuan basin has double layer magnetic structure. Two
20 earthquakes are occurred in the crust of Sichuan basin.

21 3. The different focal mechanism and geodynamics of two earthquakes may be
22 constrained by the irregular basement shape of the Sichuan Basin.

23

24 **Abstract**

25 Although many velocity and electrical models have been proposed in the
26 Longmenshan fault zone (LFZ) and its neighboring areas, the deep structure of
27 seismic gap and the geodynamics of two different earthquakes remain uncertain.
28 Based on aeromagnetic and gravity data, the Sichuan basin shows two NE-trending
29 banded and strong positive magnetic anomalies and high Bouguer gravity anomalies.
30 The banded magnetic anomalies represent the Neoproterozoic magmatic events in the
31 center of Sichuan basin, rather than the rigid Neoproterozoic and Paleoproterozoic
32 crystalline basement. The Songpan-Ganzi fold belt (SGFB) is weak positive magnetic
33 and low Bouguer gravity anomalies. The LFZ is the boundary of two anomaly areas
34 but similar to the feature of Sichuan basin. Three models are created by 2D magnetic
35 and gravity forward modeling and provide more reliable and integrated geophysical
36 interpretation for the deep structure of earthquake epicenter and seismic gap. The
37 models reveal that the crust of Sichuan basin consists of double layer magnetic
38 basement. More importantly, the basement subducted to about 33km west of the
39 Wenchuan-Maoxian fault with low dip angle beneath the middle segment of the LFZ,
40 whereas the distance decrease to about 17 and 19 km under the south segment. So, the
41 crust of Sichuan basin beneath the middle segment extends further than the one
42 beneath the south segment with the seismic gap as transition zone. Therefore, we
43 propose the irregular shape of basement in western margin of Sichuan basin maybe
44 the main reason for the different focal mechanism and geodynamic of Wenchuan and
45 Lushan earthquakes.

46 **Keywords:** aeromagnetic and gravity, crustal structure, seismic gap, Longmenshan
47 fault zone, Wenchuan earthquake, Lushan earthquake, geodynamics

48

49 **1. Introduction**

50 In 2008 and 2013, the devastating Wenchuan Mw 7.9 and Lushan Ms7.0
51 earthquakes struck the LFZ along the eastern margin of the Tibetan Plateau
52 successively. The two events caused great losses to human lives and property in China.

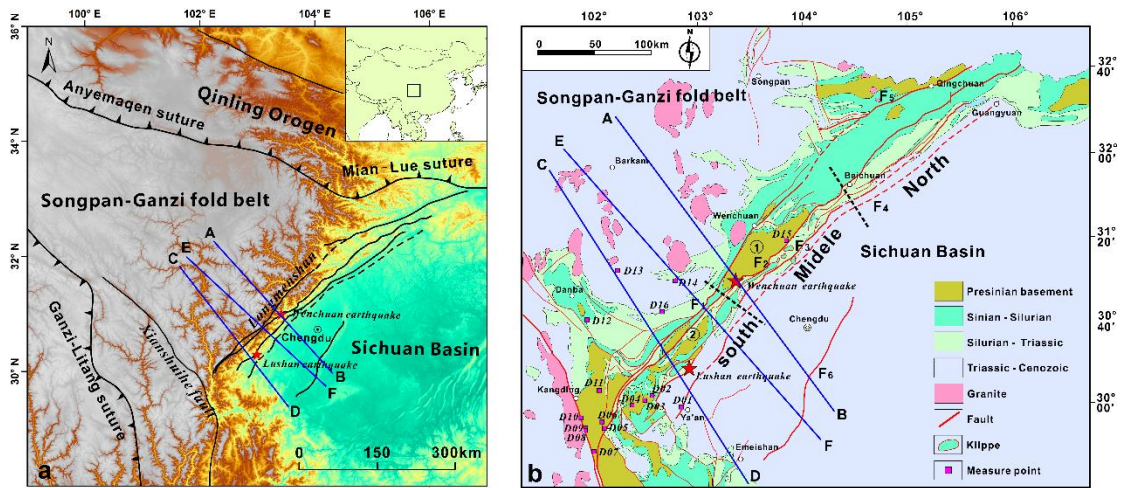
53 A lot of researches involving the focal mechanism, coulomb failure stress and deep
54 structure have been carried out in this area in order to find the relation between the
55 two events and potential seismic hazard area along the LFZ. There are at least four
56 differences between the two events: (1) The Wenchuan earthquake occurred in the
57 Yingxiu-Beichuan fault in the middle section of the LFZ, while the Lushan
58 earthquake occurred in a blind reverse fault east of the Shuangshi-Dachuan fault in
59 the south segment (Li et al., 2013; Wang et al., 2014a; Chen et al., 2013), (2) The
60 Wenchuan Earthquake is thrust faulting associated with a dextral strike-slip with
61 surface rupture extending over 300 km toward NE (Chen et al., 2013). The Lushan
62 Earthquake is dominated by pure thrust faulting with the rupture zone restricted in 30
63 km underground and no obvious surface rupture (Zhao et al., 2013; Chen et al., 2013),
64 (3) The Lushan earthquake is located in the area where the Coulomb stress increased
65 after the Wenchuan earthquake (Wu et al., 2013; Shan et al., 2013; Wang et al.,
66 2017b), (4) High velocity (V_p , V_s), low Poisson's ratio, and high resistivity were
67 determined at the 2013 Lushan hypocenter, whereas high velocity (V_p , V_s), high
68 Poisson's ratio and high resistivity were imaged at the 2008 Wenchuan hypocenter
69 (Lei and Zhao, 2010; Pei et al., 2010; Wang et al., 2009, 2015; Zhan et al., 2013). The
70 key issue has been shifted to deep structure of seismic gap since the Lushan
71 earthquake took place because these differences are constrained by an approximately
72 50km wide seismic gap. The recent achievements suggest the deep of seismic gap
73 exist low velocity (V_p , V_s), high Poisson's ratio and high conductivity materials
74 interpreted as a fluid-bearing ductile crust (Pei et al., 2014; Wang et al., 2015; Liu et
75 al., 2018). However, the formation of seismic gap and geodynamic of two earthquakes
76 with different focal mechanism is still unclear (Teng et al., 2014; Wang et al., 2013;
77 Chen et al., 2013; Xu et al., 2013; Wu et al., 2016) .

78 As we known, the uplift of LFZ is controlled by the interaction of Yangtze block
79 and Tibet Plateau. The crustal structure of Yangtze block plays an important role in
80 the thrusting and deformation of the LFZ because the Yangtze block as a rigid and
81 stable Craton prevents the eastward expansion of the Tibetan Plateau. However, we
82 still know a little about the structure of Yangtze block beneath the eastern Tibet
83 Plateau because of thick sedimentary cover and less geophysical data. The

84 geodynamic process of the LFZ and its constraint on the genesis of two different
85 earthquakes remain uncertain. Several models have been proposed regarding the
86 different emplacement styles of Yangtze block under the eastern Tibet Plateau (Guo et
87 al., 2013; Yin et al.,2010); (1) Underthrusting of the Yangtze crust beneath the
88 Songpan-Ganzi terrane (Clark et al.,2005; Jiang and Jin, 2005), (2) Indentation of the
89 Yangtze crust beneath the Songpan-Ganzi terrane (Cai et al.,1996; Zhang et al.,2004).
90 (3) Yangtze crystalline crust including rigid and highly thrust portion extending
91 beneath the eastern most Tibetan Plateau to the LRQF (Guo et al., 2013). These
92 models are insufficient to explain the difference between two earthquakes due to the
93 lack of detail crustal image along the LFZ. The purpose of this study is to provide
94 more information on crustal structure beneath the middle and south segment of LFZ
95 by 2D forward modeling of aeromagnetic and gravity data, and to give another
96 perspective for understanding of the deep structure and geodynamic of LFZ.

97 **2. Tectonic setting**

98 The LFZ is formed by a series of parallel imbricate thrust fault with strike of
99 NE-SW, the transition zone of Songpan-Ganzi fold belt and Sichuan Basin (Fig. 1a).
100 This belt is bounded by the Mianxian-Lueyang suture (abbreviated to Mian-Lue
101 suture) to the north and Xianshuihe fault to the south. There are four main reversed
102 thrust and strike-slip faults from NW to SE, including the Wenchuan - Maowen Fault
103 (F1), the Yingxiu - Beichuan Fault (F2), the Pengxian - Guanxian (Pengguan) Fault
104 (F3), and Guangyuan - Dayi concealed fault (F4) (Figure 1b). The fault zone can be
105 divided into three segments along the strike with the boundary of Beichuan-Anxian
106 and Wolong-Huaiyuan. The north segment developed imbricate thrust fault system in
107 front of outcropped Proterozoic Jiaoziding complex and Tangwangzhai syncline. The
108 middle and south segments are characterized by the outcrop of Proterozoic Pengguan
109 and Baoxing complex respectively. Both of them developed klippe along the front of
110 the complexes. The geological observation suggests the time of deformation is getting
111 younger, the deformation is more brittle and extensive, and the Cenozoic activity is
112 more intense from northeast to southwest along the LFZ (Li et al., 2008) . The
113 Wenchuan earthquake is located in the middle segment of the LFZ, while the Lushan
114 earthquake lies in south segment.



116

117 Fig.1 (a) Topographic map of the eastern Tibetan Plateau and Sichuan basin, showing
 118 the location of modeling profiles as blue lines. (b) Geological map of the LFZ
 119 (modified after Li et al., 2008 and Yan et al., 2011).

120 F₁: Wenchuan-Maoxian fault, F₂: Yinxiu-Beichuan fault, F₃: Pengxian-Guanxian fault,
 121 F₄: Guangyuan-Dayi concealed fault, F₅: Pingwu-Qingchuan fault, F₆: Longquanshan
 122 fault; ① Pengguan complex; ② Baoxing complex

123

124 The strata are successive distributed from Proterozoic to Cenozoic in the LFZ.
 125 These outcrops record a lot of messages for tectonic evolution of the LFZ and provide
 126 important information for understanding the concealed basement in Sichuan basin. In
 127 order to study the aeromagnetic anomaly in the LFZ and surrounding areas, the
 128 magnetic susceptibility is measured for different kinds of rocks with each point test
 129 for 30 times. The result shows Proterozoic serpentine has the strongest magnetism
 130 with the average magnetic susceptibility value of $7645 \times 10^{-5} \text{SI}$. Proterozoic quartz
 131 diorite has moderate magnetic susceptibility of $2381-4873 \times 10^{-5} \text{SI}$ with an average
 132 value of $3774 \times 10^{-5} \text{SI}$, while Proterozoic granite is $20-2466 \times 10^{-5} \text{SI}$ with an average
 133 value of $679 \times 10^{-5} \text{SI}$. The Triassic and Jurassic granite is widely distributed in the
 134 west of the LFZ, the magnetic susceptibility is $1179-2012 \times 10^{-5} \text{SI}$, and the average
 135 value is $1670 \times 10^{-5} \text{SI}$. The magnetic susceptibility of Siguniangshan granite is
 136 $767-1614 \times 10^{-5} \text{SI}$ with the average value of $1231 \times 10^{-5} \text{SI}$. Most sedimentary strata are
 137 non-magnetic except for the formations consisting of volcanic rocks. In general, the

138 outcropped Proterozoic medium-acidic intrusive rocks are commonly strong
 139 magnetism.

140 **Table 1** Statistic of rock magnetic susceptibility in the LFZ

Period	lithologic	min	max	average	Point No.
Neoproterozoic	quartz diorite	2255	5617	4069	D04
Neoproterozoic	granite	8	285	50	D05
Neoproterozoic	granite	132	816	405	D06
Neoproterozoic	granite	94	477	318	D07
Neoproterozoic	granite	1349	3590	2466	D08
Neoproterozoic	quartz diorite	157	5417	2381	D09
Neoproterozoic	quartz diorite	1440	8677	4873	D10
Neoproterozoic	granite	153	2239	819	D11
Neoproterozoic	Serpentine (Not in-suit)	4903	12030	7645	D15-1
Neoproterozoic	granite	8	77	20	D15
Devonian	Mica schist	710	8401	2497	D12
Permian	Basalt (Not in-suit)	615	7099	3613	D16
Triassic	granite	460	2387	1179	D02
Triassic	granite	1053	2587	1820	D03
Triassic	Syenite (Not in-suit)	1215	2428	2012	D13
Jurassic	granite	767	1614	1231	D14
Cretaceous	Mudstone	25	180	106	D01

141

142 **3. Method**

143 **3.1 Aeromagnetic data processing method**

144 The aeromagnetic data used in this study are collected from Chinese 1/5,000,000
 145 aeromagnetic maps that compiled by China Aero Geophysical Survey and Remote
 146 Sensing Center for Natural Resource (Xiong et al., 2013). The data grid is 1km×1km
 147 with the flight height set to 1km. Due to the effect of tilt magnetization, the magnetic
 148 anomaly center may not correspond to the location of geological body. Therefore, the
 149 frequency-domain dipole-layer changing inclination method is conducted for
 150 reduction to the pole to reduce the influence caused by the change of latitude (Xiong
 151 et al., 2013). In order to separate anomalies caused by deep-sourced magnetic bodies,
 152 upward continuation is performed through setting observation surface to 20km above
 153 the ground surface. Meanwhile, vertical first derivative calculation is used to study the

154 distribution of shallow geological bodies and structures.

155 **3.2 Two-dimensional (2D) forward modeling**

156 Based on the previous seismic profile, the sequential modeling of the original
157 gravity and aeromagnetic data afforded reasonable interpretation results as opposed to
158 model each data individually. Velocity can not only provide Moho distribution and
159 crustal layering for initial model, but also guiding for density modeling by
160 speed-density empirical calculation formula (Christensen and Mooney, 1995; Brocher,
161 2005). Then physical properties of different rocks were modeled, magnetic
162 susceptibility contrast for aeromagnetic data and density for gravity data. So, the
163 linked modeling of the three datasets produced integrated and less ambiguous results.
164 Meanwhile, this method can easily add priori geological and structural information
165 and the understanding of geologists to increase the interpretability of the model.

166 The models were created using 2D gravity/magnetic interactive modeling
167 package running on GM-SYS Program, through Oasis Montaj Programs. The
168 sequential gravity-magnetic modeling was done first by defining the depths to upper,
169 middle, lower crust and Moho discontinuities from seismic image. The density values
170 of initial model referred from the previous density structure in the Longmenshan area
171 and were constrained by the seismic velocity results (Wang et al., 2014b; Zhang et al.,
172 2014). The initial magnetic susceptibility was given by the measured data. The
173 magnetic susceptibility of basement rock in Sichuan basin referred the outcropped
174 Proterozoic intrusive rocks in the LFZ. Then the position, shape, dimensions, and
175 physical property contrast of basement rock were adjusted to get the best fit between
176 the observed and calculated data.

177 **4. Aeromagnetic and gravity anomaly feature**

178 **4.1 Aeromagnetic anomaly feature**

179 The aeromagnetic ΔT anomaly map shows that the magnetic anomaly feature
180 of the Sichuan Basin is obviously different from the SGFB, Youjiang Basin, and
181 Qinling Orogen (Fig. 2a). The Sichuan Basin is mainly characterized by NE-trending

182 banded positive and negative magnetic anomalies with large scale and high intensity.
183 The positive anomalies are mostly 200-400nT, and the negative anomalies can reach
184 -300nT. According to the magnetic susceptibility measurement results of the exposed
185 basement rock in the LFZ, the Proterozoic granites and diorite have strong magnetism
186 with the average value of $679 \times 10^{-5} \text{SI}$ and $3774 \times 10^{-5} \text{SI}$ respectively. Therefore, the
187 concealed basement rocks of the Sichuan basin causing large scale banded
188 aeromagnetic anomalies may infer as the Proterozoic igneous rocks belt that some of
189 them were outcropped on the surface by the thrusting of the LFZ. The SGFB and
190 Youjiang basin present a weak and wide positive anomaly with an anomaly intensity
191 of 10-60nT. The Qinling Orogen shows two distinct magnetic features. The eastern
192 Qinling Orogen is linear distributed positive magnetic anomalies which are bounded
193 by the Mian-Lue suture to the south, while the western Qinling is weak and negative
194 magnetic anomalies with the Anyemaqen and Mian-Lue sutures bounded to the south.
195 The sutures are usually characterized by beaded positive magnetic anomalies along a
196 certain strike, because the mafic and ultramafic rocks emplaced along the active
197 margin are strong magnetism, such as the Ganzi-Litang, Mian-Lue and Anyemaqen
198 sutures. The Xianshuihe fault plays an important role in adjusting and absorbing the
199 eastward extrusion of the Tibet Plateau. It is a sinistral strike slip fault separating
200 Youjiang basin and Sichuan basin with different magnetic anomaly feature.

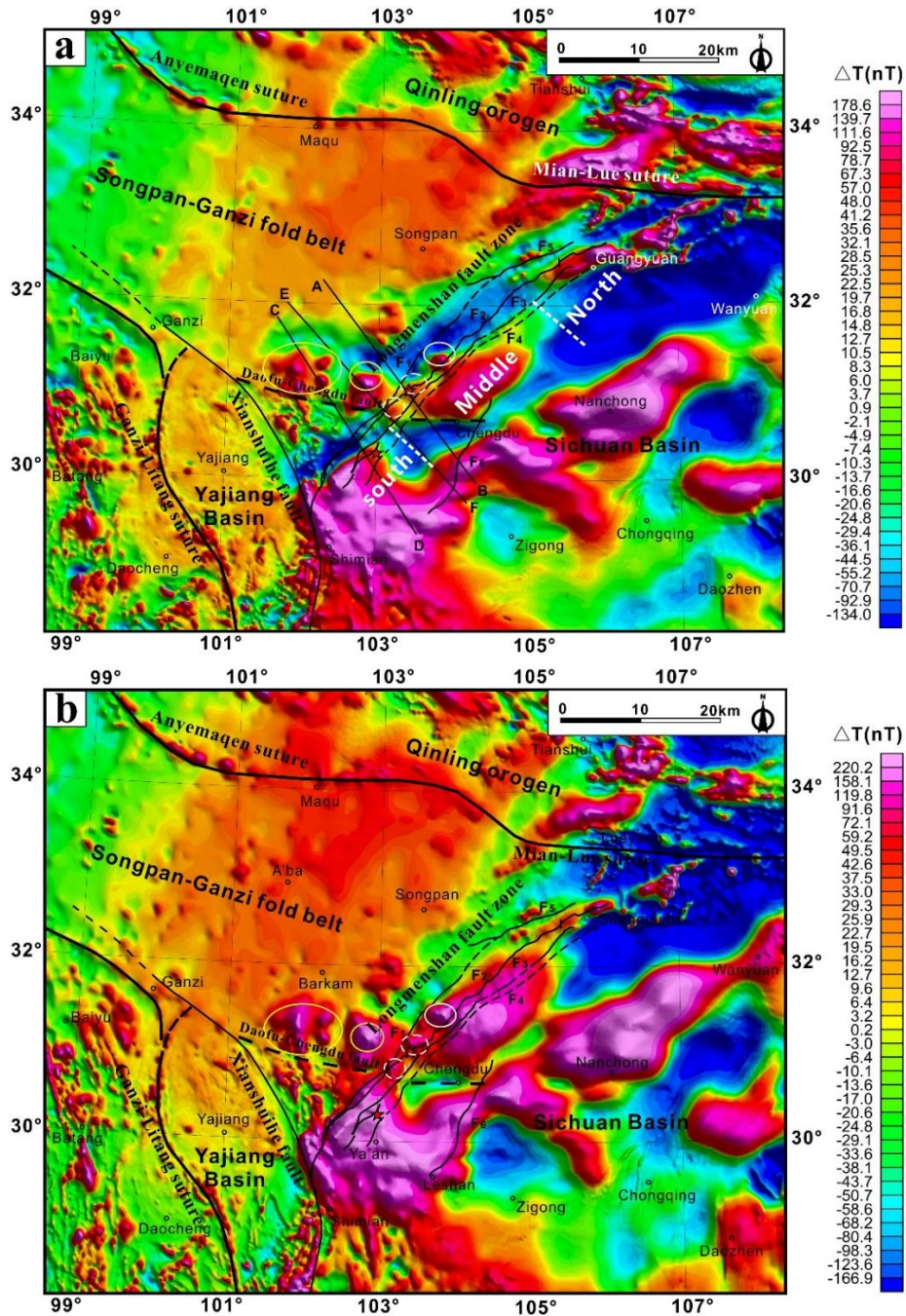
201 The magnetic anomaly feature of the LFZ is totally different from the
202 Xianshuihe fault and sutures in this area. It is characterized by gradient zone of strong
203 positive and negative anomalies that is more similar to the magnetic feature of the
204 Sichuan basin in the ΔT image (Fig.2a). According to the processing of reduction to
205 the pole, the positive anomalies in Sichuan basin shifted toward north and their
206 associated negative anomalies disappeared (Fig.2b). The LFZ lies in the banded
207 positive anomalies that produced by rigid basement of Sichuan basin. Therefore, the
208 location of fault zone on the surface is not consistent with the magnetic boundary of
209 Sichuan basin and SGFB which is in the northwest of the LFZ. This result strongly
210 suggests the LFZ thrusts above the basement of the Sichuan Basin causing the uplift
211 of Longmenshan Mountain. More importantly, according to the anomaly feature of

212 the ΔT anomaly image, the fault zone could be divided into the south, middle, and
213 north segments along the strike with the boundary of Xiling-Qionglai and
214 Nanba-Wulian. The south and middle sections are mainly characterized by positive
215 magnetic anomalies and associated negative anomalies, but they are not continuous
216 with the boundary of Xiling-Qionglai. The seismic gap is just located between two
217 discontinuous magnetic anomalies. The north segment shows small scale linear
218 magnetic anomaly zone on the negative background field. In addition, The
219 Longquanshan fault (F6) doesn't break the magnetic anomaly of crystalline basement
220 in the central of Sichuan basin, which suggests it is a shallow structure responding to
221 the thrust and napping of the LFZ.

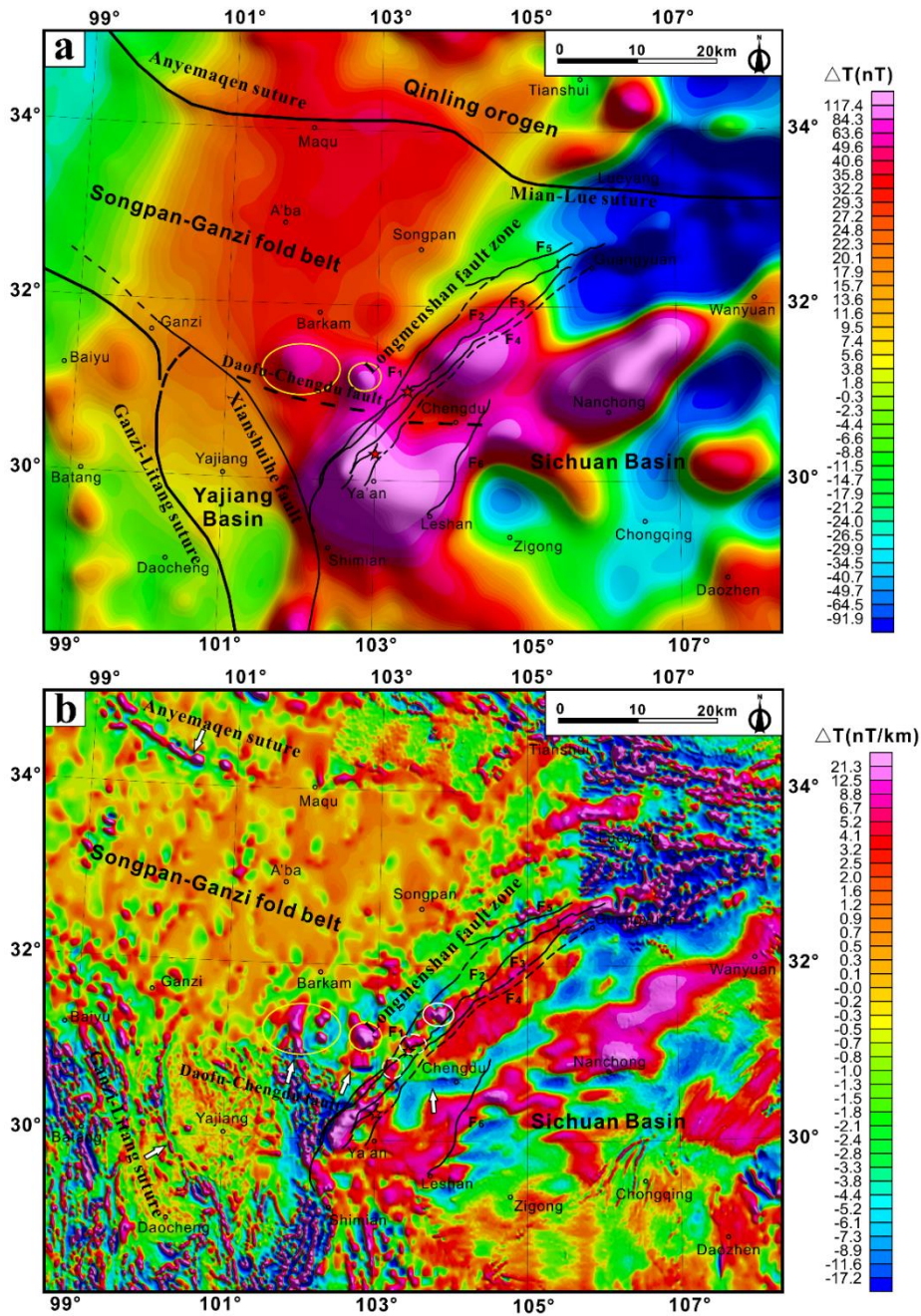
222 After 20km upward continuation of RTP image, magnetic anomalies caused by
223 ultrabasic rock in the western Sichuan Basin have disappeared and are replaced by the
224 magnetic anomalies of Sichuan basin (Fig.3a). The banded magnetic anomalies are
225 connecting with each other and form a huge magnetic block. The Siguniangshan and
226 Danba granite showing obvious positive anomalies in upward continuation image
227 suggest that these plutons have large scale and buried depth. Both the Wenchuan
228 earthquake and the Lushan earthquake occurred on the edge of the banded strong
229 magnetic anomaly (Yan et al., 2016), but the Lushan earthquake was closer to the
230 center of the magnetic body than the Wenchuan earthquake.

231 There is an obvious magnetic boundary from Daofu, Danba to Chengdu, which
232 separates two distinct magnetic anomaly areas (Fig.2a). This boundary is divided into
233 two parts by the Longmenshan fault zone in the middle. It is inferred as a concealed
234 fault that the west segment merges into the Xianshuihe fault, and the east segment
235 extends into the Sichuan Basin. The west segment is distributed along
236 Ganzi-Danba-Daxuetang where the magnetic anomaly features are totally different on
237 both sides. The magnetic anomalies on the north side of the fault are mainly caused by
238 Triassic and Jurassic granites and syenites, and the one on the south side is mainly
239 caused by strata consisting of volcanic rocks. The east segment lies in
240 Xilingzhen-Dayi-Chengdu which is characterized by the linear discontinuity of
241 magnetic anomalies. The change happened in the weak or non-magnetic basement

242 with relatively negative magnetic anomaly. Therefore, the EW-trending linear
 243 discontinuity is not clear on the ΔT and RTP image, but it is obvious on the vertical
 244 first derivative image of RTP aeromagnetic ΔT data (Fig.3b). The small change
 245 suggest that the fault is possibly formed by the differential uplift of the weak magnetic
 246 basement in Sichuan basin.



247
 248 Fig.2 (a) Aeromagnetic ΔT anomaly image of the LFZ and adjacent area, (b)
 249 Reduction to the pole (RTP) image of aeromagnetic ΔT data in the Longmenshan
 250 and adjacent area.

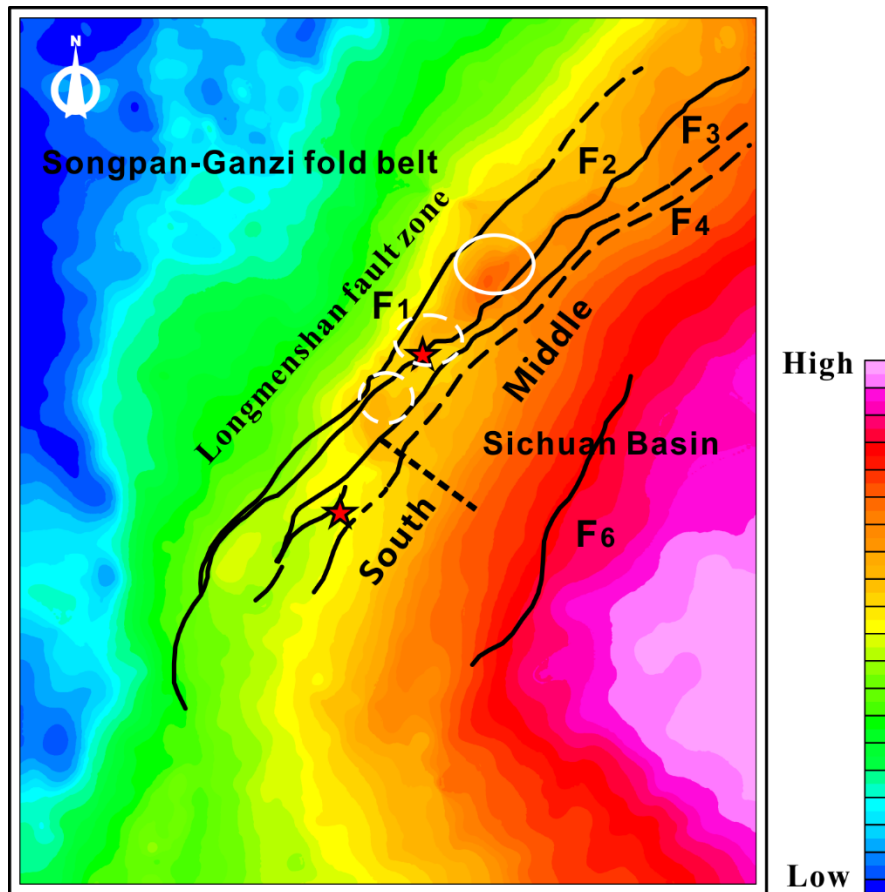


251
 252 Fig.3 (a) 20km upward continuation image of RTP aeromagnetic ΔT data in
 253 Longmenshan and adjacent area, (b) Vertical first derivative image of RTP
 254 aeromagnetic ΔT data in Longmenshan and adjacent area

255 4.2 Bouguer gravity anomaly feature

256 According to the 1/500,000 bouguer gravity anomaly image (Fig. 4), the Sichuan
 257 Basin shows high bouguer gravity anomaly with value ranging from -185 to -90 mgal.
 258 The SGFB is relatively low bouguer gravity anomaly with value of -435 to -250 mgal.
 259 The LFZ is characterized by gradient zone between two blocks with a gravity value of

260 -290 to -185 mgal. Obviously, the crust of Sichuan basin has a higher density than the
 261 one in Songpan-Ganzi fold belt. The gravity anomaly feature in the LFZ is similar
 262 with the anomaly produced by the basement of the Sichuan Basin. More importantly,
 263 the gravity anomaly feature also could be divided into two segments along the fault
 264 strike with the boundary of Xiling-Qionglai. The bouguer gravity value of middle
 265 segment is -250~-185mgal, while the southern segment is -290~-215mgal. The
 266 segmentation of the LFZ through gravity anomaly is consistent with result divided by
 267 magnetic anomaly on the aeromagnetic ΔT image. The epicenter of Wenchuan
 268 earthquake is located in a relatively high gravity anomaly area with the value ranging
 269 from -215 to -225 mgal, while the Lushan earthquake is low gravity value of -250 to
 270 -260 mgal. The seismic gap is a transition zone where the epicenters of two
 271 earthquakes on both sides show different gravity anomaly features.
 272



273
 274 Fig.4 Bouguer gravity anomaly image of Longmenshan and adjacent area.
 275

276 **5. 2D forward modeling results of the LFZ**

277 In recent years, a lot of seismic imaging works have been published to discuss
278 the velocity structure of earthquake epicenters and seismic gap (He et al., 2017; Liu et
279 al., 2018). Three S-wave velocity models are founded by receiver function method
280 based on the seismic data acquired from 57 temporary and fixed seismic station (He et
281 al., 2017). These models show clearly S-wave velocity change beneath the epicenter
282 of two earthquakes and the seismic gap. In order to gain a reliable model of crustal
283 structure in the LFZ, three S-wave velocity profiles were used to constrain the 2D
284 magnetic and density modeling. The calculated models first provide magnetic and
285 density information beneath the Longmenshan and adjacent areas.

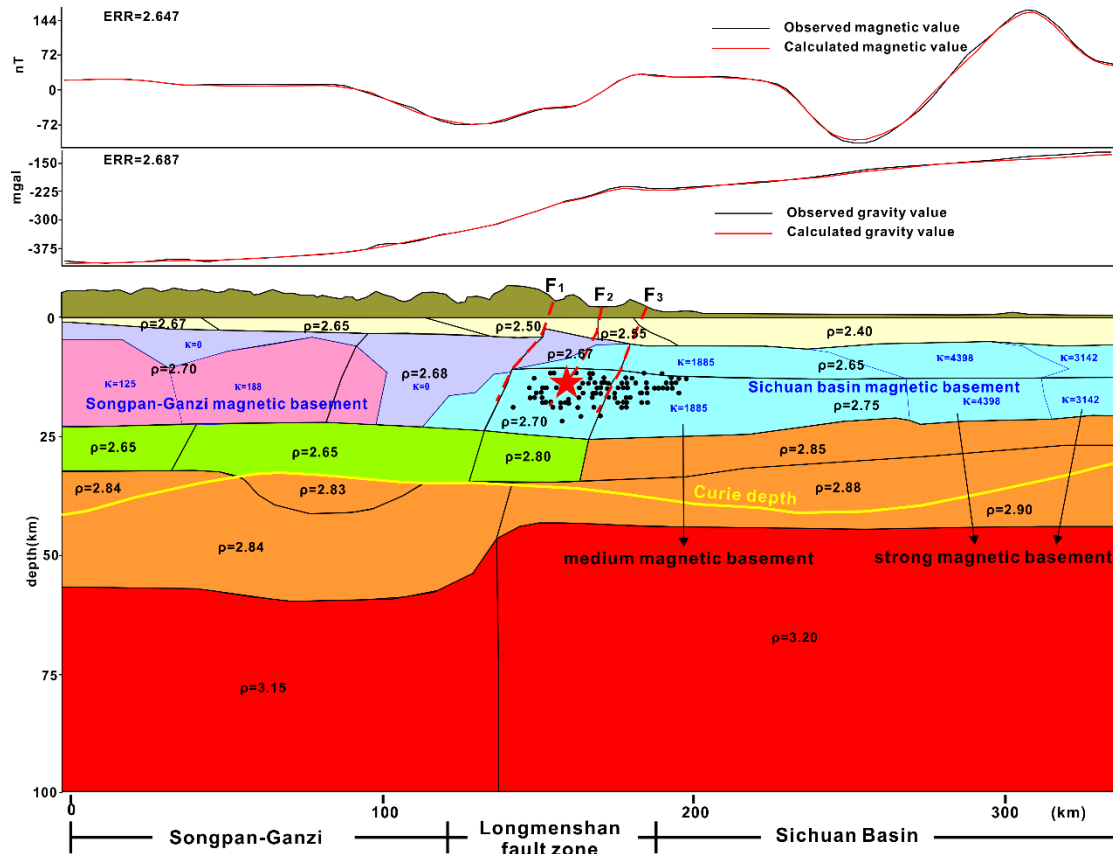
286 **(1) Profile AB**

287 Profile AB passed through epicenter of Wenchuan earthquake (Fig. 5). The
288 southeast of the profile shows strong magnetic and high gravity anomaly values
289 suggesting the basement of Sichuan basin is strong magnetic and high density. The
290 SGFB is relatively weak magnetic and low density. The modeling results indicate the
291 magnetic susceptibility and density of magnetic basement are $1885-4398 \times 10^{-5} \text{SI}$ and
292 $2.65-2.75 \text{g/cm}^3$ respectively in Sichuan basin. The depth to the top of the magnetic
293 basement is 5-7 km, and the thickness is about 15-20 km. The thickness of magnetic
294 basement is stable in the basin, but it gradually thins through the LFZ and disappeared
295 near Lixian. In contrast, the values are $125-188 \times 10^{-5} \text{SI}$ and $2.68-2.70 \text{g/cm}^3$ in
296 Songpan-Ganzi area respectively. The depth to the top of basement is about 4-10km,
297 and thickness is 12-18km. There is a non-magnetic area between two basements with
298 low density, which is a vertical low-velocity zone that extends downward to the
299 crustal low-velocity zone in the V_s model. This zone is probably a weak and
300 brittleness area formed by the collision of Sichuan Basin and the Songpan-Ganzi fold
301 belt.

302 The model indicates the crust of Sichuan basin is double-layer magnetic
303 structure. Strong magnetic basement have high average magnetic susceptibility of

304 3142-4398×10⁻⁵SI in the southeast end of the profile, which is corresponded to the
305 NE-trending positive magnetic anomaly belt in the central of Sichuan basin on the
306 aeromagnetic ΔT image. The basement dips to southeast. The medium magnetic
307 basement extends beneath the LFZ from central Sichuan basin with an average
308 magnetic susceptibility of 1885×10⁻⁵SI. The medium magnetic layer is covered by the
309 strong one. Moreover, there is a magnetic body with thickness of 16 km under the
310 strong magnetic anomaly zone in the middle of Sichuan Basin with a magnetic
311 susceptibility of 4398×10⁻⁵SI, which infers to the Proterozoic igneous rocks.
312 Meanwhile, Deep seismic reflection profile shows that there is a paleo subduction
313 zone preserved in the middle of the Yangtze Craton with the depth about 42km (Gao
314 et al.,2016; Wang et al., 2017a).

315 The LFZ is clearly the boundary of gravity anomaly in the profile, but not for the
316 magnetic anomaly. The gravity value is slightly increased in the Longmenshan area,
317 which could be well modeled by the uplift of high density geological body to the
318 shallow surface through the thrust of the LFZ. The modeling magnetic basement of
319 the Sichuan Basin obviously extends beneath the LFZ, which displays a high velocity
320 zone in the Vs model (He et al., 2016). The gravity value decreases rapidly from
321 Yinxiu-Beichuan fault to northwest, but the higher gravity value than the northwest
322 end of profile may also shows the influence of the subducted basement. Moreover, the
323 front edge of the magnetic basement is consistent with the rigid basement of the
324 Yangtze crust given by the deep seismic reflection profile (Guo et al., 2013). The
325 result strongly suggests the basement of the Sichuan Basin has been subducted to the
326 west of the Wenchuan-Maoxian fault. The low-velocity zone of the middle-upper
327 crust extends below the magnetic basement of the Sichuan Basin. The Wenchuan
328 earthquake and its aftershocks are distributed inside the rigid magnetic basement of
329 the Sichuan basin above the front of low-velocity layer.



330

331 Fig.5 Two-dimensional gravity and magnetic model and interpreted crustal structure
 332 along the seismic profile AB. ρ marks density with the unit of g/cm^3 , κ marks
 333 magnetic susceptibility with the unit of 10^{-5}SI . Black line is the boundary of density
 334 block, blue line is the boundary of magnetic block.

335

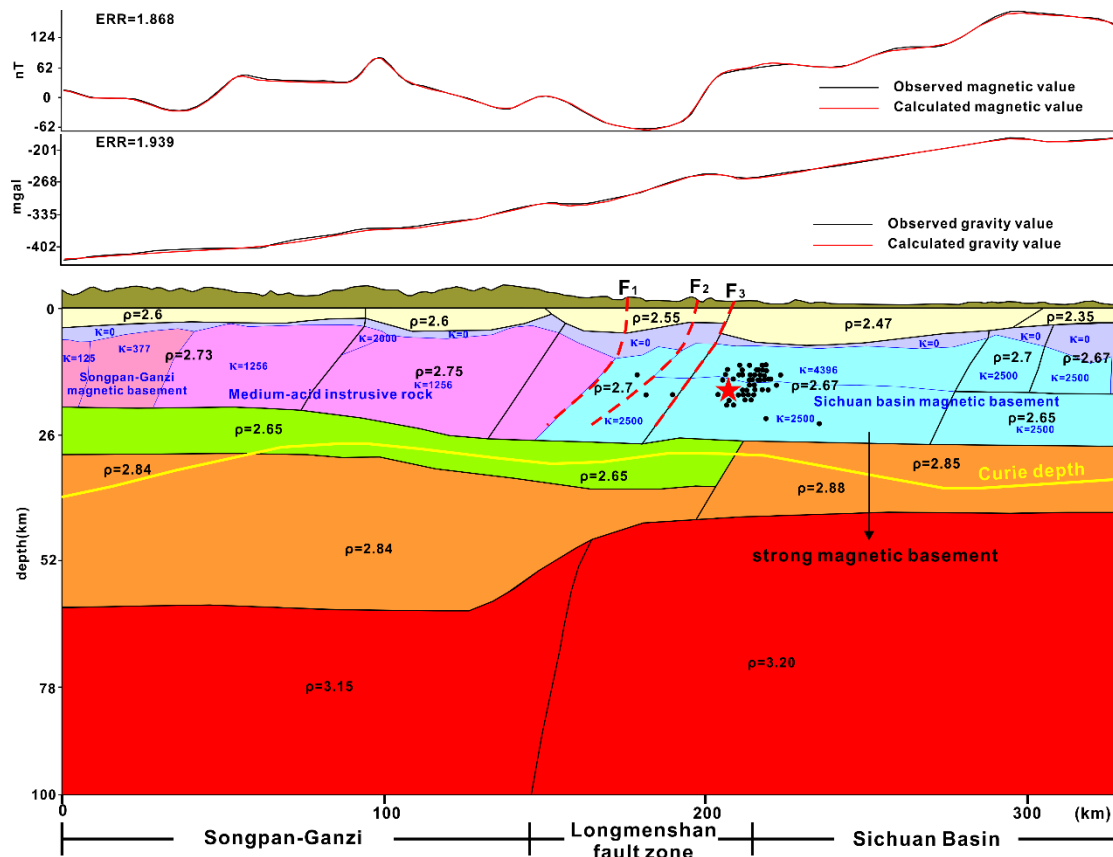
336 **(2) Profile CD**

337 Profile CD passes through the epicenter of Lushan earthquake (Fig.6). In contrast
 338 to the profile AB, the bouguer gravity anomaly value gradually decreases from
 339 Sichuan basin to SGFB without obvious change through the LFZ. The values only
 340 slightly increase in the Longmenshan area, which are produced by the uplift of high
 341 density geological body. However, the magnetic anomaly values show big change on
 342 the both side of the LFZ. The values are high in the Sichuan basin and decrease
 343 rapidly in the LFZ. Therefore, the modeling result shows the basement of the Sichuan
 344 Basin is strong magnetism with magnetic susceptibility of $2500\text{-}4396 \times 10^{-5}\text{SI}$. The
 345 density is $2.65\text{-}2.70\text{g/cm}^3$. The magnetic layer dip to the northwest. The depth to the
 346 top of magnetic basement is about 5-11km, and the thickness is about 17-23km. The

347 magnetic layer thins from northwest to the middle of the basin and reaches about
348 17km in the middle. Meanwhile, there is a magnetic body with medium magnetic
349 susceptibility of 1256×10^{-5} SI in the west of Wenchuan-Maoxian fault. The depth to
350 the top of the magnetic body is 3-6km, and the thickness is 16-20km. The density is
351 $2.73-2.75 \text{g/cm}^3$. The magnetic body is inferred as extensive medium-acid intrusive
352 rocks formed in the west margin of Sichuan basin, because there are many Triassic
353 and Jurassic granite, syenite, and granodiorite plutons outcropped on the surface with
354 certain magnetism. The basement of SGFB has low magnetic susceptibility of
355 $125-377 \times 10^{-5}$ SI in the northwest end of the profile. The depth to the top of the
356 magnetic basement is about 4-7km, and the thickness is about 13-16km.

357 The magnetic basement of Sichuan basin also extends beneath the LFZ, but the
358 subduction distance and occurrence are different from profile AB. For instance, there
359 is no double layer magnetic structure in this profile. The magnetic basement subducts
360 beneath the LFZ with a low angle and thins immediately in profile AB. However, the
361 basement shows a high angle under the LFZ in profile CD. And, the top of magnetic
362 basement shows large fluctuation. The result suggests the crystalline basement is
363 highly thrust and deformed in the southwest margin of Sichuan basin. The
364 low-velocity layer in the middle-upper crust extends below the magnetic basement of
365 the Sichuan Basin. The Lushan earthquake and its aftershocks are distributed inside
366 the rigid magnetic basement of the Sichuan Basin above the low-velocity layer.

367



368

369 Fig.6 Two-dimensional gravity and magnetic model and interpreted crustal structure
 370 along the seismic profile CD. ρ marks density with the unit of g/cm^3 , κ marks
 371 magnetic susceptibility with the unit of 10^{-5}SI . Black line is the boundary of density
 372 block, blue line is the boundary of magnetic block.

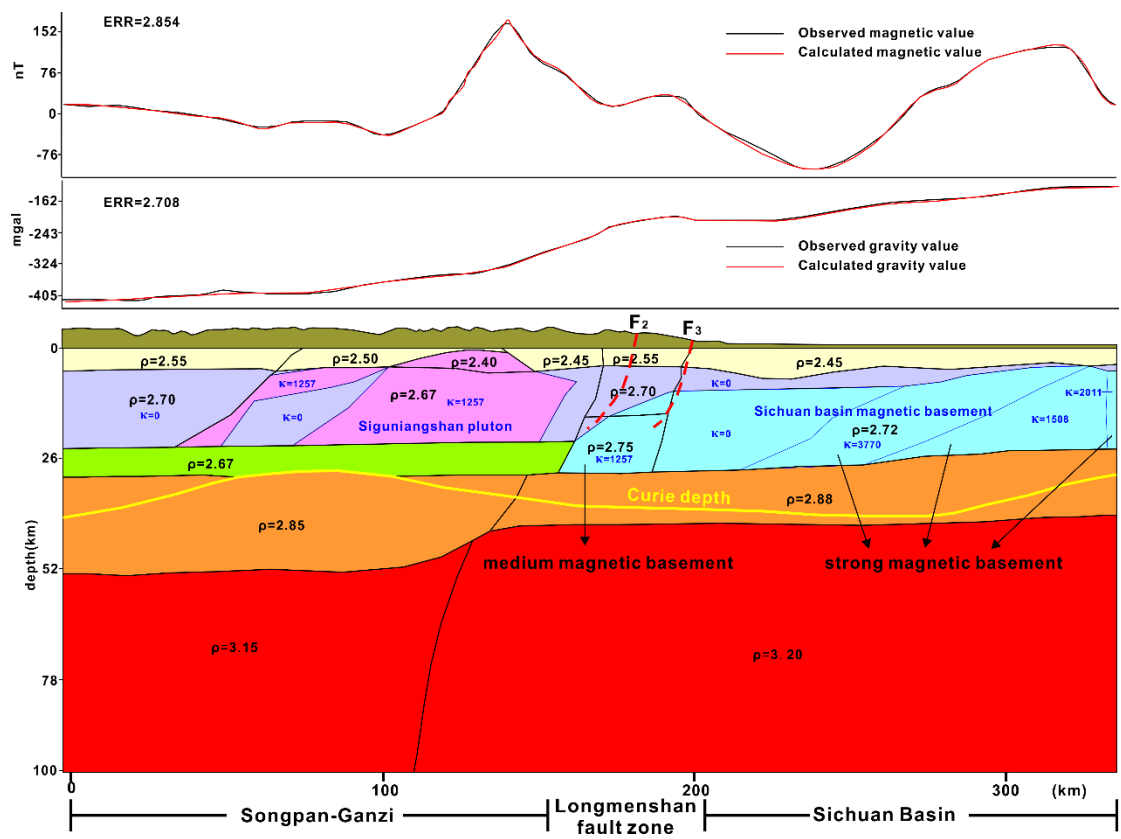
373

374 (3) Profile EF

375 Profile EF passes through seismic gap (Fig.7). The bouguer gravity anomaly
 376 values show obvious change from Sichuan basin to SGFB with the boundary of the
 377 LFZ. The values slightly increase in the Longmenshan area, which are produced by
 378 the uplift of high density geological body. The magnetic anomaly values also show
 379 big change. The basement of Sichuan basin shows double layer magnetic structure,
 380 which is the same as profile AB. The strong magnetic basement distributes in the
 381 middle of Sichuan basin with the magnetic susceptibility of $1508\text{-}3770 \times 10^{-5}\text{SI}$. The
 382 depth to the top of the magnetic basement is 4-10km, and the thickness is about
 383 15-19km. The medium magnetic basement is locally distributed beneath the
 384 Longmenshan area with a magnetic susceptibility of $1257 \times 10^{-5}\text{SI}$. The thickness

385 gradually decreases and disappears in the west of the Beichuan-Yingxiu fault.
 386 However, the contact of double-layer magnetic basement does not show the feature
 387 that strong magnetic basement covers the medium one directly as in profile AB. A
 388 large area of non-magnetic sedimentary cover or basement is distributed between the
 389 two magnetic layers. Moreover, the strong magnetic basement dips to northwest,
 390 rather than the southeast in profile AB.

391 The magnetic anomaly values increase rapidly in the northwest of the LFZ,
 392 which is caused by the outcropped Siguniangshan granite with magnetic susceptibility
 393 of $1257 \times 10^{-5} \text{SI}$. The modeling result shows the pluton extends downward to the
 394 low-velocity zone of the middle-upper crust from surface and the thickness is about
 395 22km. The magnetic basement under the Longmenshan area of this profile does not
 396 have a complex thrust and nappe structure like the previous two profiles. The
 397 low-velocity layer in the middle and upper crust doesn't extend below the magnetic
 398 basement in the Sichuan Basin.



399
 400 Fig.7 Two-dimensional gravity and magnetic model and interpreted crustal structure
 401 along the seismic profile EF. ρ marks density with the unit of g/cm^3 , κ marks

402 magnetic susceptibility with the unit of 10^{-5} SI. Black line is the boundary of density
403 block, blue line is the boundary of magnetic block.

404 **6. Discussion**

405 **6.1 The basement of Sichuan basin**

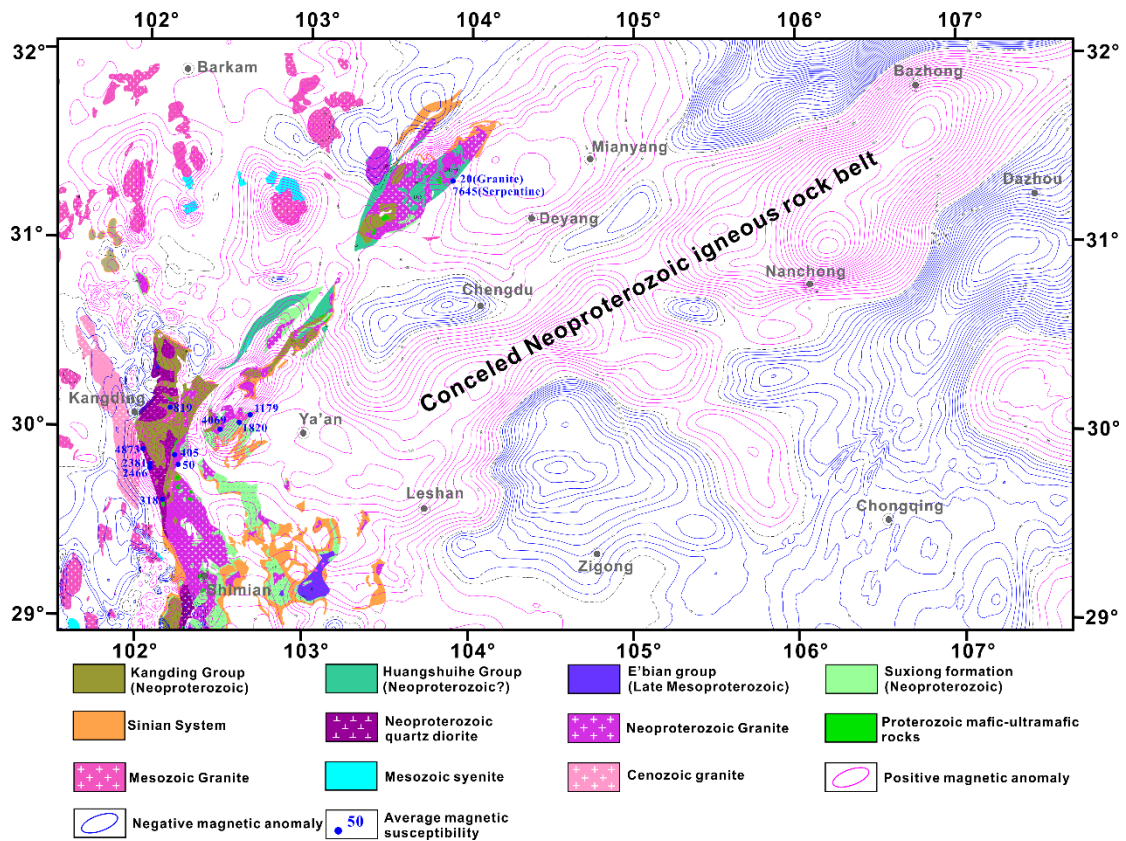
406 The result not only provides 2D magnetic and density information for the crust of
407 Sichuan basin, but also the geometry of different geological unit. The characteristics
408 of gravity and magnetic anomaly are totally different between Sichuan Basin and
409 SGFB. The Sichuan Basin shows NE-trending banded positive and negative magnetic
410 anomalies with intensity ranging from -200 to 300 nT. The magnetic anomalies
411 become large scale magnetic block after 20 km upward continuation. The feature
412 suggests the geological bodies produced the anomalies are large scale and deep source.
413 The Sichuan Basin also has high Bouguer gravity values ranging from -185 to
414 $-90 \times 10^{-5} \text{m/s}^2$. The aeromagnetic field in the Songpan-Ganzi region is reflected as a
415 broad positive and negative anomaly area with low anomaly intensity of $-40 \sim 40 \text{nT}$.
416 When the magnetic data is conducted upward continuation to 20 km, the magnetic
417 anomaly shows the same feature. The SGFB is relatively low bouguer gravity
418 anomaly with value of -435 to -250 mgal. The results indicate the crust of SGFB is
419 weak magnetic and low density compared with the crust of Sichuan basin.

420 Based on the understanding of previous geological survey, the basement rocks are
421 mainly composed of Neoproterozoic - Paleoproterozoic crystalline basement and Meso-
422 to Neoproterozoic folded basement in Sichuan basin (SBGMR, 1991). The
423 Neoproterozoic-Paleoproterozoic crystalline rock is represented by the Kangding group
424 with high grade metamorphism. The Meso- and Neoproterozoic folded basement
425 rocks are represented by a sequence of low grade metamorphism strata, such as the
426 Qiasi, Yanbian, Huangshuihe, Tongmuliang, Huodiya, Huili, E'bian, Dengxiangying
427 and Lengjiayi Groups. However, a large amount of geochronological and geochemical
428 evidences have shown that the Kangding complex has arc signatures, representing
429 metamorphic products of Neoproterozoic, arc-related acidic plutons, rather than
430 Neoproterozoic and Paleoproterozoic crystalline basement (Zhou et al., 2002; Lai et al.,

431 2015; Chen et al., 2005; Du et al., 2007; Kang et al., 2017; Liu et al., 2009; Geng et al.,
432 2007). Meanwhile, a few zircon U–Pb data has shown the Huangshuihe and Yanjing
433 Groups also formed in the Neoproterozoic, and the E' bian group formed in late
434 Mesoproterozoic (Ren et al., 2013; Du et al., 2005; Chen et al., 2018). These late
435 Mesoproterozoic and Neoproterozoic assemblage outcropped in western margin of
436 Sichuan basin are well matched with the positive magnetic anomalies on RTP
437 aeromagnetic ΔT anomaly image (Fig.8). According to the field observation of
438 magnetic susceptibility, the Neoproterozoic quartz diorite usually has strong
439 magnetism, while the Neoproterozoic granites have relatively low magnetic
440 susceptibility values. Both of them could produce strong positive magnetic anomalies.
441 Therefore, the banded positive magnetic anomaly is closely related to the
442 Neoproterozoic magmatic events, rather than the present of rigid Neoproterozoic and
443 Paleoproterozoic crystalline basement in the center of Sichuan basin. The result
444 strongly suggests the Sichuan basin formed a uniform block by the converging of
445 ancient micro blocks along the concealed magmatic rock belt during Late
446 Mesoproterozoic and Neoproterozoic. The belt produced large scale banded magnetic
447 anomalies in the central of Sichuan basin.

448 More importantly, magnetic anomaly feature provides essential information for
449 spatial and temporal distribution of basement in Sichuan Basin. The calculating
450 models suggest the basement of Sichuan basin has double layer magnetic structure in
451 profile AB and EF, which indicate the basement may be formed by two blocks with
452 different rock assemblage (Fig.5 and Fig.7). The strong magnetic layer covers the
453 medium magnetic layer directly in profile AB. However, the strong magnetic layer
454 covered by non-magnetic sedimentary formation or basement, and the medium
455 magnetic layer locally distributed in the west margin of Sichuan basin in profile EF.
456 Meanwhile, there is only one layer magnetic basement in profile CD. This may
457 indicate the basement composition is different along the western margin of Sichuan
458 basin (Fig.9). More importantly, the magnetic basement wedges beneath the LFZ with
459 the distance about 33km west of Wenchuan-Maoxian fault in profile AB. The result is
460 consistent with the model inversed by magnetotelluric data (Zhu et al., 2008).

461 However, the distance is 17km and 19km in profile CD and EF. Therefore, the
 462 subducted distance of the basement has big lateral change which is the same as the
 463 composition along the western margin of Sichuan basin. The basement beneath the
 464 middle segment of the LFZ extends farther than the one under the south segment,
 465 which formed a "stair-shape" along the Longmenshan fault (Fig.9). The Wenchuan
 466 and Lushan earthquakes occurred on different step surfaces.
 467



468
 469 Fig.8 RTP aeromagnetic ΔT anomalies contour and outcrops of Precambrian
 470 basement and intrusive rocks in the western margin of Sichuan basin (modified after
 471 1:1, 000, 000 digital geological map of China (Li, 2005) and reference from Zhou et
 472 al.(2002)).

473
 474 The modeling results indicate two disastrous earthquakes and their aftershocks
 475 are mainly distributed in the magnetic basement of the Sichuan Basin (Fig.7 and
 476 Fig.9). The magnetic basement has undergone a strong deformation because the top of
 477 the layer has obvious fluctuation beneath the LFZ. Meanwhile, the thickness has

478 gradually decreased when the magnetic basement wedges in the eastern Tibet Plateau.
 479 However, the deformation of magnetic basement is not obvious beneath the seismic
 480 gap. The seismic images show the crustal low velocity zone extends beneath the
 481 epicenter of Wenchuan and Lushan earthquake, but it doesn't extend under the
 482 seismic gap (He et al., 2017). Therefore, the happening of two earthquakes may be
 483 closely related to the destruction of the magnetic basement through the detached
 484 upper crust of SGFB collision with the Yangtze's crust. The western margin of
 485 Yangtze block also shows several obvious discontinuities in the Moho surface on the
 486 seismic sounding profile (Guo et al., 2013).

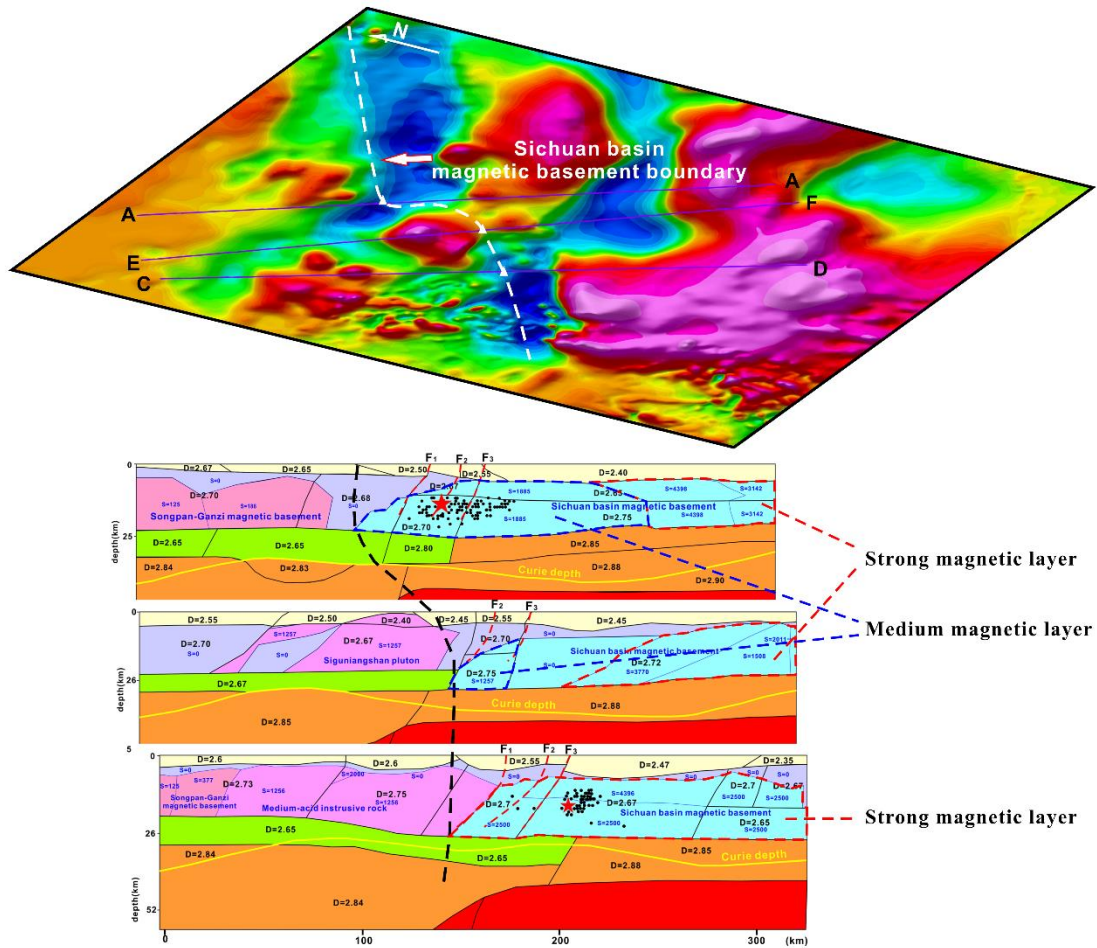


Fig.9 Western margin of magnetic basement in Sichuan basin.

6.2 Seismogenesis mechanism of the LFZ

The LFZ is the transition zone of Tibet Plateau and Yangtze Craton. A lot of

492 researches suggest the LFZ has been thrust above the Sichuan basin (Wang et al.,
493 2015; Zhu et al., 2008; Guo et al., 2013; Xiong et al., 2016). This hypothesis could be
494 well proved by magnetic and gravity data. The magnetic anomaly feature of LFZ is
495 represented by the feature of Sichuan basin, because the thrustsed sedimentary covers
496 are commonly non-magnetic. The gravity anomaly feature in the LFZ is similar with
497 the anomaly produced by the basement in the Sichuan Basin. As we known, the
498 Sichuan basin has been subducted beneath the SGFB during the Late Indosinian -
499 Early Yanshanian. The process caused partial melt of the crust and formed a series of
500 intermediate-acid intrusive rock in the SGFB. The isotope and chronology data show
501 that these rocks have Proterozoic clastic zircon cores and Nd model ages (T_{DM}),
502 which indicate there is Proterozoic Yangtze-type continental crust beneath the
503 Songpan-Ganzi area (Dai et al., 2011; Hu et al., 2005; Zhao et al., 2007a, b). The
504 modeling results confirm the basement of the Sichuan basin has extended to the west
505 of the Wenchuan-Maoxian fault and reached the deep of the SGFB. Therefore, The
506 LFZ doesn't show unique feature on the magnetic and gravity image, because it is a
507 transition zone that the crust of Sichuan basin dose exists under the SGFB.

508 The gravity and magnetic anomalies show obviously lateral change along the
509 strike of the LFZ, which could be divided in to south, middle and north segments
510 (Fig.2a and Fig.6). The south segment is characterized by the magnetic anomaly
511 gradient zone and the low Bouguer gravity anomaly, while the middle segment is the
512 magnetic anomaly gradient zone and high Bouguer gravity anomaly. The Wenchuan
513 and Lushan earthquakes are distributed in the middle and south segment respectively.
514 The boundary between the two segments is the gap with rare seismic events when two
515 earthquakes happened. The northern segment is characterized by a negative magnetic
516 field with some linear magnetic anomaly zone superimposed. The division based on
517 geophysical data is the same as the surface deformation of the LFZ (Li et al., 2008).
518 The 2D modeling results suggest the lateral change of magnetic and gravity anomaly
519 is attributed to different extending distance and formation of magnetic basement of
520 Sichuan basin beneath the LFZ. It strongly suggests that the distribution of magnetic
521 basement controls the evolution and deformation of shallow structures in western

522 margin of Sichuan basin.

523 The Wenchuan earthquake occurred in the Yingxiu-Beichuan fault, which belongs
524 to the central-front range fault system in the middle segment of the LFZ. The Lushan
525 earthquake took place in a blind reverse fault to east of the Shuangshi-Dachuan fault,
526 which belongs to the front range fault system in the south segment of the LFZ.
527 Although the two segments are separated by the seismic gap with small distance, the
528 geological deformation is quite different. The front range structure in the southern
529 segment is much more complicated than that in the middle segment. Meanwhile, the
530 range of latest structural deformation increases from 30km in the middle segment to
531 150km in the south segment (Xu et al., 2013). The focal mechanism shows the
532 Lushan earthquake is a pure thrust event without obvious rupture on both sides (Chen
533 et al., 2013). The axis of the maximum horizontal stress lies in NW-SE (Luo et al.,
534 2015). However, the Wenchuan Earthquake is dominated by thrusts with a dextral
535 strike-slip component. The surface rupture mainly extends toward northeast with the
536 distance about 300km. The axis of the maximum horizontal stress presents several
537 different directions (Luo et al., 2015). These features indicate that the deformation
538 mechanism of the middle and south segment is different. High-resolution geodetic
539 data shows the surface deformation has obvious change on the both side of seismic
540 gap (Wang et al., 2011). Therefore, this study proposes the differences for the focal
541 mechanism of the two earthquakes may be closely related to differential thrusting
542 mechanism caused by the irregular basement shape in the western margin of the
543 Sichuan Basin.

544 Both earthquakes and their aftershocks occurred in the rigid magnetic basement
545 of the Sichuan Basin, where is characterized by high velocity area in seismic image
546 (Wang et al., 2015). There is a seismic gap with low V_p and V_s , high Poisson's ratio,
547 and high conductivity between the two earthquakes. It is inferred as a fluid-rich
548 ductile crust extending to the middle and lower crust (Pei et al., 2014; Zhan et al.,
549 2013; Wang et al., 2015). According to the modeling result, the seismic gap also has
550 magnetic basement. But the magnetic anomalies appear discontinuity along Xiling
551 Town-Dayi-Chengdu, which is inferred as a fault zone that cut the basement of

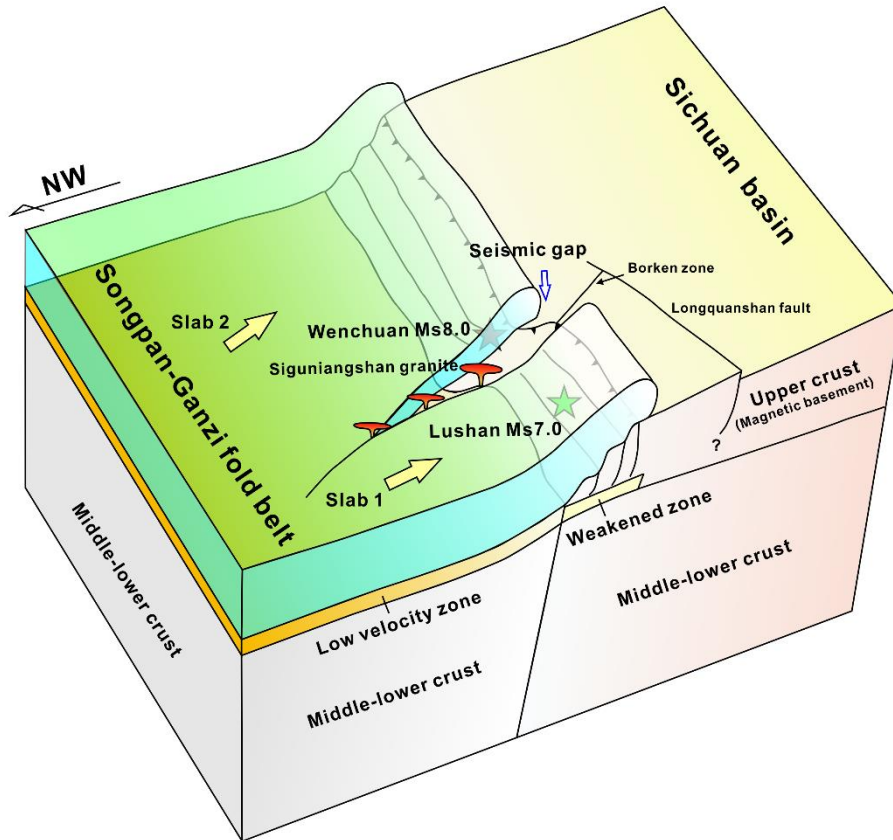
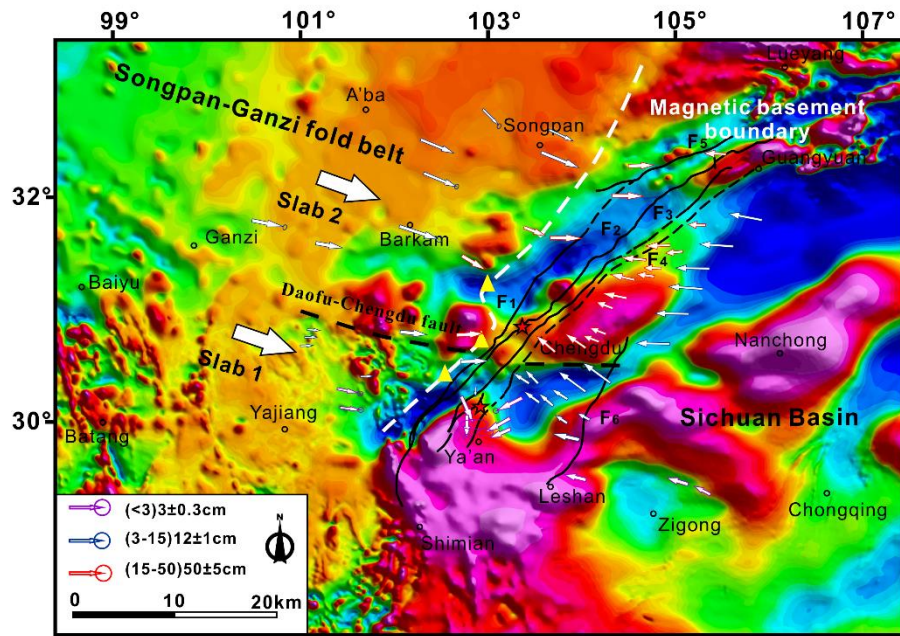
552 Sichuan basin. Because the sedimentary covers are commonly non-magnetic in
553 Sichuan basin that could not cause the change of magnetic anomaly. The magnetic
554 anomaly decays obviously after 5km upward continuation, which suggests the
555 displacement is small between the hanging wall and foot wall. The fault cuts the
556 magnetic anomaly and extends to Longquanshan Mountain. The seismic result shows
557 the ductile crust extend 20-30km in deep and cuts the crust of Sichuan basin (Wang et
558 al., 2015; He et al., 2017) . The fault may be closely related to the early activities of
559 Longmenshan fault and the uplift of Longquanshan Mountain.

560 This contributes proposed a schematic model (Fig.10). The rigid basement of the
561 Sichuan Basin wedges beneath the Songpan-Ganzi fold belt during Late
562 Indochina-early Yanshanian. The basement beneath the middle and north segment of
563 the LFZ wedges further than the one under the south segment. The lateral change of
564 the basement could cause the Songpan-Ganzi fold belt to tear into two pieces with
565 different mechanic system (slab 1 and slab 2 in Fig.10). Different mechanical systems
566 lead to different activities of the two slabs that forms a series of extension
567 environment for the emplacement of intermediate and acid intrusive rocks. This
568 tectonic framework has been preserved until now. With the continuous uplift of the
569 Tibet Plateau, the compression stress is increasing in the western margin of Sichuan
570 basin. In 2008 and 2013, two earthquakes with different focal mechanism happened
571 successively in the middle and south segment of the LFZ. Two earthquakes are
572 located in the different basement of Sichuan basin. The Lushan earthquake was
573 blocked by the irregular basement of the Sichuan Basin and the Siguniangshan pluton
574 to the northeast, and was constrained by the Xianshuihe fault to the southwest. But the
575 Wenchuan earthquake only was controlled by the Siguniangshan pluton to the
576 southwest. Apparently, the central Sichuan basin maybe involved in the early thrust
577 process of the south segment of the LFZ, which is represented by the displacement of
578 basement and uplift of Longquanshan Moutain.

579

580

581

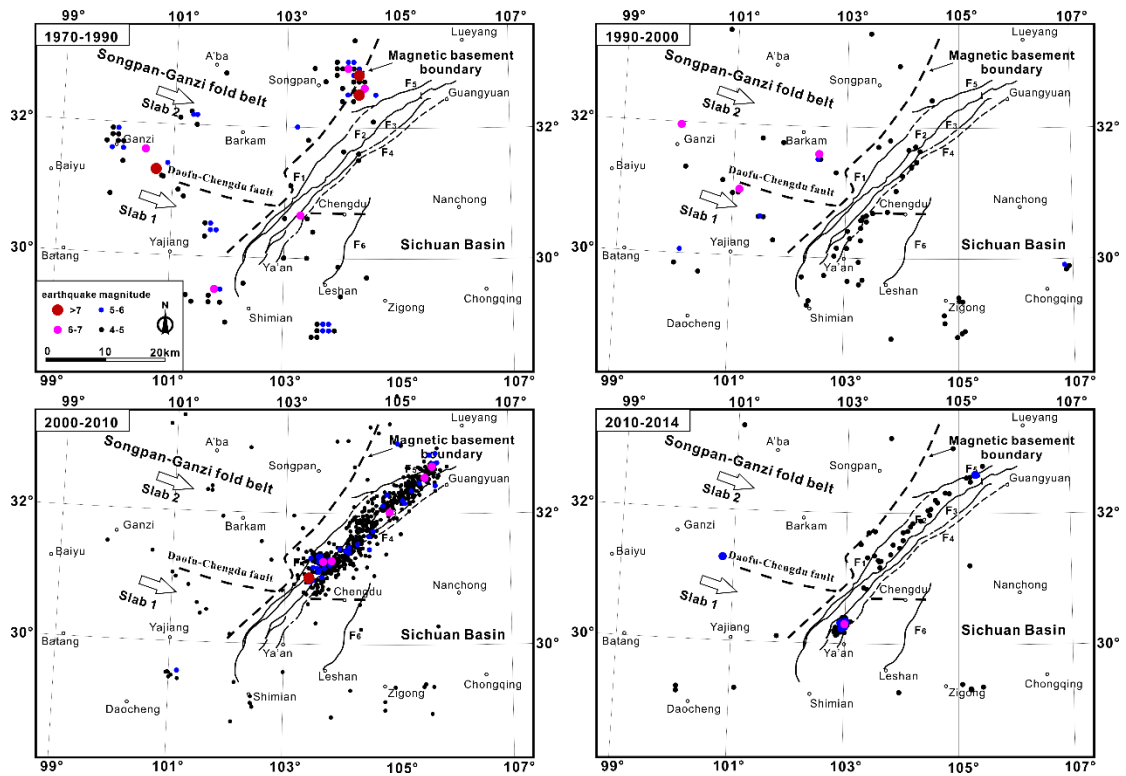


582

583 Fig.10 Schematic deep structure model of Longmenshan and adjacent area

584 The earthquake catalogs are collected from the China Earthquake Networks
 585 Center (CENC). The statistical result shows earthquake distribution in Longmenshan
 586 area since 1970 with the magnitude above four (Figure 11). It should be noted that
 587 there were almost no earthquakes in the southern segment of the LFZ when the

588 Wenchuan earthquake occurred. However, a lot of earthquakes happened in the
 589 middle-north segment when the Lushan earthquake occurred. The results show that
 590 the stress mainly accumulated in the middle and north segment of the LFZ before the
 591 Wenchuan earthquake. After the Wenchuan earthquake taken place, the stress began to
 592 increase in the south segment until the Lushan earthquake was triggered. A lot of
 593 studies prove that the Coulomb stress in the southern segment of the LFZ began to
 594 increase after the Wenchuan earthquake occurred (Wang et al., 2014c; Jia et al., 2014;
 595 Shan et al., 2013; Parsons et al., 2008; Yi et al., 2013). The difference of stress
 596 accumulation may be related to the different wedging distance of Yangtze's crust
 597 beneath the middle and south segment of LFZ.
 598



599
 600 Fig.11 Distribution of earthquakes (magnitude ≥ 4) in Longmenshan area since 1970
 601

602 Our interpretation of two earthquakes is as follows:

603 (1) With the uplift of Tibet Plateau, The Songpan-Ganzi block continued to
 604 move toward the southeast and first colliding with the basement of the Sichuan Basin
 605 beneath the middle-north segment of the LFZ. Stress accumulated in the middle-north

606 segment and triggered the Wenchuan Ms7.9 earthquake. Due to the obstruction of
607 emplaced Siguniangshan pluton, there was no large scale surface rupture presented to
608 the southwest of the Wenchuan earthquake. But the rupture extended about 340km
609 toward northeast.

610 (2) The compression stress was completely released in the middle and north
611 sections of the LFZ after the Wenchuan earthquake occurred, which was represented
612 by large-scale surface rupture and dextral strike-slip. Meanwhile, the compression
613 stress shifted to the south segment and finally triggered the Lushan Ms7.0 earthquake.
614 Due to the constraints of Yangtze's irregular crust and Xianshuihe fault on both sides,
615 the Lushan earthquake was a pure thrust event without obvious rupture on both sides.
616 There were some residual compression stresses still work in the middle-north segment,
617 few earthquakes with low magnitude have been observed.

618 **7. Conclusion**

619 This study found the difference of gravity and magnetic anomaly between
620 middle and south segment of the LFZ. Then 2D forward modeling was conducted
621 under the constraint of the previous seismic image in this area. Three
622 magnetic-density models were constructed, which passed through epicenter of
623 Wenchuan and Lushan earthquake and seismic gap respectively. The result first
624 proposes the basement of Sichuan basin beneath the middle segment is different from
625 the one beneath the south segment. The basement has double layer magnetic structure
626 and wedges beneath the middle segment of LFZ with a long distance and low dip
627 angle. However, the basement is one layer magnetic structure and wedges beneath the
628 south segment with a short distance and high dip angle. The magnetic basement
629 involves in more intense deformation beneath the epicenter of two earthquakes than
630 the seismic gap. Due to the irregular morphology of the basement and emplaced
631 intermedium-acid intrusive rocks, the thrust mechanism is different in middle and
632 south segment of the LFZ. It provides essential tectonic framework for the genesis of
633 the two earthquakes with different focal mechanism. Meanwhile, the early thrust
634 process in the south segment of the LFZ also caused the differential uplift of the

635 basement on both side of Diya-Chengdu fault. This contribute provides some new
636 geophysical evidence for mapping the deep structure of the LFZ. It is of great
637 significance to study the genesis of earthquakes in the LFZ.

638 **Acknowledgement**

639 Thanks to the anonymous reviewers for their hard work and constructive
640 comments. Thanks to Professor Chuntao Liang and Fujun He from Chengdu
641 University of Technology for providing Seismic imaging results and enthusiastic help.
642 Thanks to all colleagues for their hard work. Aeromagnetic data for this study were
643 provided by China Aero Geophysical Survey and Remote Sensing Center for Natural
644 Resource (<http://www.agrs.cn/>). Gravity data were provided by Development
645 Research Center of China Geological Survey (<http://www.drc.cgs.gov.cn/>). The 2D
646 models were created by the program Geosoft Oasis Montaj
647 (<https://www.sequent.com/products-solutions/geosoft-oasis-montaj/>). This research
648 was funded by the China Geological Survey Project (202012000000180102) and
649 Youth Innovation Fund Program of AGRS (2016YFL05).

650 **References**

- 651 Brocher, T.M. (2005). Empirical Relations between Elastic Wave speeds and Density in the Earth's
652 Crust. *Bulletin of the Seismological Society of America*, 95(6):2081-2092.
- 653 Chen, F.L., Xie, Y., Cui, X.Z., Sun, Z.M., Ren, G.M., & Deng, Q. (2018). Geochronology,
654 geochemistry and tectonic implications of basalts from the Ebian Group in the western
655 Yangtze block, South China. *J. Mineral Petrol.*, 38, 76-86.
- 656 Chen, G.X. (2012). The study of magnetic correspondence analysis over Longmen Mountain
657 tectonic belt and adjacent areas. Xi'an: Northwest University. (in Chinese with English
658 abstract)
- 659 Chen, L.C., Ran, Y.K., Wang, H., Li, Y.B., & Ma, X.Q. (2013). The Lushan Ms7.0 earthquake and
660 activity of the southern segment of the Longmenshan fault zone. *Chin. Sci. Bull.*, 58, 3475–
661 3482.
- 662 Chen, Y.L., Luo, Z.H., Zhao, J.X., Li, Z.H., Zhang, H.F., & Song, B. (2005). Petrogenesis and
663 dating of the Kangding complex, Sichuan province. *Science in China Series D: Earth
664 Sciences*, 48, 622–634.
- 665 Christensen, N.I., & Mooney, W.D. (1995). Seismic velocity structure and composition of the
666 continental crust: A global view. *Journal of Geophysical Research*, 100, 9761-9788.
- 667 Dai, Z.M., Sun, C.M., Zhang, K.Z., Li, & Z.J. (2011). U-Pb dating of zircons from the Four-Girl
668 Mountain Pluton in the Songpan-Garzê Terrane, and the relationship between the pluton and
669 the Wenchuan Ms8.0 Earthquake of 2008. *China Geology*, 38, 111-124. (in Chinese with

670 English abstract)

671 Du, L.L., Geng, Y.S., Yang, C.H., Wang, X.S., Ren, L.D., Zhou, X.W., et al. (2005). Geochemistry
672 and SHRIMP U–Pb zircon chronology of basalts from the Yanbian Group in the Western
673 Yangtze Block. *Acta Geologica Sinica*, 79, 805–813 (in Chinese with English abstract).

674 Du, L.L., Geng, Y.S., Yang, C.H., Wang, X.S., Zhou, X.W., Ren, L.D., et al. (2007). New
675 understanding on Kangding Group on western margin of Yangtze Block: evidence from
676 geochemistry and chronology. *Acta Geologica Sinica*, 81, 1562–1577 (in Chinese with
677 English abstract).

678 Gao, R., Chen, C., Wang, H.Y., Lu Z.W., Brown, L., Dong, S.W., et al. (2016). SINOPROBE deep
679 reflection profile reveals a Neo-Proterozoic subduction zone beneath Sichuan Basin. *Earth
680 and Planetary Science Letters*, 454:86-91.

681 Geng, Y.S., Yang, C.H., Wang, X.S., Ren, L.D., Du, L.L., & Zhou, X.W., (2007a). Age of
682 crystalline basement in western margin of Yangtze Block. *Geological Journal of China
683 Universities*, 13, 429–441 (in Chinese with English abstract).

684 Guo, X.Y., Gao, R., Randy Keller, G., Xu, X., Wang, H.Y., & Li, W.H. (2013). Imaging the crustal
685 structure beneath the eastern Tibetan Plateau and implications for the uplift of the Longmen
686 Shan range. *Earth and Planetary Science Letters*, 379, 72-80.

687 He, F.J., Liang, C.T., Yang, Y.H., Fang, L.H., & Su, J.R. (2017). The crust structure of the
688 unruptured segment between Wenchuan and Lushan earthquake revealed by receiver
689 functions. *Chinese Journal of Geophysical*, 60, 2130-2146. (in Chinese with English abstract)

690 Hu, J.M., Meng, Q.R., Shi, Y.R., & Qu, H.J. (2005). SHRIMP U-Pb dating of zircons from
691 granitoid bodies in the Songpan-Ganzi terrane and its implications. *Acta Petrologica Sinica*,
692 21, 867-880. (in Chinese with English abstract)

693 Jia, K., Zhou, S.Y., Zhuang, J.C., & Jiang, C.S. (2014). Possibility of the Independence between
694 the 2013 Lushan Earthquake and the 2008 Wenchuan Earthquake on Longmen Shan Fault,
695 Sichuan, China. *Seismological Research Letters*, 85(1):60-67.

696 Kang H., Li D.P., Chen Y.L., Hu G.Q., & Deng W.B. (2017). Origin and tectonic implications of
697 Kangding intrusive complexes in Sichuan Province: Evidence from zircon Hf isotope.
698 *Geology in China*, 44(6): 1175-1189 (in Chinese with English abstract).

699 Lai, S.C., Qin, J.F., Zhu, R.Z., & Zhao, S.W. (2015). Neoproterozoic quartz monzodiorite–
700 granodiorite association from the Luding–Kangding area: Implications for the interpretation
701 of an active continental margin along the Yangtze Block (South China Block). *Precambrian
702 Research*, 267, 196-208.

703 Lei, J., & Zhao D. (2010), Structural heterogeneity of the Longmenshan fault zone and the
704 mechanism of the 2008 Wenchuan earthquake (Ms 8.0), *Geochem. Geophys. Geosyst.*, 10(10),
705 1-17. doi:10.1029/2009GC002590.

706 Li, H.M. (2012). The study of magnetic structure over Longmen Mountain tectonic belt and its
707 adjacent areas. Xi'an: Northwest University. (in Chinese with English abstract)

708 Li, T.D. (2017). 1:1000000 geological map of China. The Institute of Geology, Chinese Academy
709 of Geological Sciences. doi: 10.23650/data.H.2017.NGA105570.T1.64.1.

710 Li, Y.Q., Jia, D., Wang, M.M., Shaw, J.H., He, J.K., Lin, A.M., et al. (2014), Structural geometry
711 of the source region for the 2013 Mw 6.6 Lushan earthquake: Implication for earthquake
712 hazard assessment along the Longmen Shan, *Earth Planet. Sci. Lett.*, 390, 275–286.

713 Li, Z.W., Liu, S.G., Chen, H.D., Liu, S., Guo, B., Tian, X.B. (2008). Structural segmentation and

- 714 zonation and differential deformation across and along the Longmen thrust belt, West
715 Sichuan, China. *Journal of Chengdu University of Technology (Science & Technology*
716 *Edition)*, 35, 440-454. (in Chinese with English abstract)
- 717 Liu, S.W., Yan, Q.R., Li, Q.G., & Wang, Z.Q. (2009a). Petrogenesis of granitoid rocks in the
718 Kangding Complex, western margin of the Yangtze Craton and its tectonic significance. *Acta*
719 *Petrologica Sinica*, 25, 1883–1896 (in Chinese with English abstract).
- 720 Liu, Z.Q., Liang, C.T., Hua, Q., Li, Y., Yang, Y.H., He, F.J., & Fang, L.H. (2018). The seismic
721 potential in the seismic gap between the Wenchuan and Lushan earthquakes revealed by the
722 joint inversion of receiver functions and ambient noise data. *Tectonics*, 37, 4226-4238.
- 723 Luo, Y., Zhao, L., Zeng, X.F., & Gao, Y. (2015). Focal mechanisms of the Lushan earthquake
724 sequence and spatial variation of the stress field. *Science China Earth Science*,
725 58(7),1148-1158.
- 726 Parsons, T, Chen, J, & Kirby, E. (2008). Stress changes from the 2008 Wenchuan earthquake and
727 increase hazard in the Sichuan basin. *Nature*, 454: 509–510.
- 728 Pei, S., Su, J., Zhang, H., Sun, Y., Toksoz, M., Wang, Z., Gao, X., et al. (2010), Three-dimensional
729 seismic velocity structure across the 2008 Wenchuan Ms 8.0 earthquake, Sichuan, China,
730 *Tectonophysics*, 491, 211–217.
- 731 Pei, S.P., Zhang, H.J., Su, J.R., & Cui, Z.X. (2014). Ductile Gap between the Wenchuan and
732 Lushan Earthquakes Revealed from the Two-dimensional Pg Seismic Tomography. *Scientific*
733 *Reports*, 4, 6489
- 734 Ren, G.M., Pang, W.H., Sun, Z.M., & Yin, F.G. (2013). Zircon SHRIMP U-Pb dating of basalt
735 from Huangshuihe Group on the western margin of the Yangtze block and its geological
736 significance. *Geology in China*, 40, 1007-1015. (in Chinese with English abstract)
- 737 Sichuan Bureau of Geology and Mineral Resources (SBGMR). (1991). Regional Geology of
738 Sichuan Province. Beijing: Geological Publishing House. (in Chinese).
- 739 Shan, B., Xiong, X., Zheng, Y., Jin, B.K., Liu, C.L., Xie, Z.J., & Hsu, H.T. (2013). Stress changes
740 on major faults caused by 2013 Lushan earthquake and its relationship with 2008 Wenchuan
741 earthquake. *Science China Earth Science*, 56, 1169-1176.
- 742 Tang, X.G., You, S.S., Hu, W.B., & Yan, L.J. (2012). The crustal density structure underneath
743 Longmenshan fault zone. *Seismology and Geology*, 34, 28-38. (in Chinese with English
744 abstract)
- 745 Teng, J.W., Bai, D.H., Yang, H, Yan, Y.F., Zhang, H.S., Zhang, Y.Q., & Ruan, X.M. (2008). Deep
746 processes and dynamic responses associated with the Wenchuan Ms8.0 earthquake of 2008.
747 *Chinese J. Geophys.*, 51, 1385-1402. (in Chinese with English abstract)
- 748 Wang, H.Y., Gao, R., Lu, Z.W., Li, W.H., Guo, H., Xiong, X.S., et al. (2017a). Deep crustal
749 structure in Sichuan basin: Deep seismic reflection profiling. *Chinese Journal of Geophysical*,
750 60, 2913-2923. (in Chinese with English abstract)
- 751 Wang, J.J., Xu, C.J., Freymueller, J. T., & Li, Z.H. (2017b). Probing Coulomb stress triggering
752 effects for a Mw N 6.0 earthquake sequence from 1997 to 2014 along the periphery of the
753 Bayan Har block on the Tibetan Plateau. *Tectonophysics*, 694, 249-267.
- 754 Wang, M., Jia, D., Shaw, J.H., Hubbard, J., Plesch, A., Li, Y., & Liu, B. (2014a). The 2013 Lushan
755 earthquake: Implications for seismic hazards posed by the Range front blind thrust in the
756 Sichuan Basin China, *Geology*, 42, 915–918.
- 757 Wang, P., Zhang, Z.J., Zhang, X., Han, Y.Y., Wang, M.L., Hou, J., & Xu, T. (2014b). Crustal

758 density structure of the central Longmenshan and adjacent area and its geodynamic
759 implications. *Acta Petrologica Sinica*, 30, 1179-1187. (in Chinese with English abstract)

760 Wang, Q., Qiao, X.J., Lan, Q.G., Jeffrey, F., Yang, S.M., Xu, C.J., et al. (2011). Rupture of deep
761 faults in the 2008 Wenchuan earthquake and uplift of the Longmen Shan. *Nature Geoscience*,
762 4, 630-640.

763 Wang, W.M., Hao, J.L., & Yao, Z.X. (2013). Preliminary result for rupture process of Apr.20, 2013,
764 Lushan Earthquake, Sichuan, China. *Chinese Journal of Geophysical*, 56, 1412-1417. (in
765 Chinese with English abstract)

766 Wang, Y.Z., Wang, F., Wang, M., Shen, Z.K., & Wan, Y.G. (2014c). Coulomb stress change and
767 evolution induced by the 2008 Wenchuan earthquake and its delayed triggering of the 2013
768 Mw6.6 Lushan earthquake. *Seismological Research Letter*, 85, 52-59.

769 Wang, Z., Y. Fukao, & S. Pei (2009), Structural control of rupturing of the Mw7.9 2008 Wenchuan
770 Earthquake China, *Earth Planet. Sci. Lett.*, 279, 131–138.

771 Wang, Z., Su, J.R., Liu, C.X., & Cai, X.L. (2015). New insights into the generation of the 2013
772 Lushan Earthquake (Ms 7.0), *China. J. Geophys. Res. Solid Earth*, 120, 3507–3526.

773 Wu, M.L., Zhang, C.Y., & Fan, T.Y. (2016). Stress state of the Baoxing segment of the
774 southwestern Longmenshan Fault Zone before and after the Ms 7.0 Lushan earthquake.
775 *Journal of Asian Earth Sciences*, 121, 9–19.

776 Wu, Y.Q., Jiang, Z.S., Wang, M. Chen, S., Liao, H., Li, Q., et al. (2013). Preliminary results
777 pertaining to coseismic displacement and preseismic strain accumulation of the Lushan Ms
778 7.0 earthquake as reflected by GPS surveying. *Chinese Science Bulletin*, 58, 3460-3466.

779 Xu, X.W., Chen, G.H., Yu, G.H., Cheng, J., Tan, X.B., Zhu, A.L., & Wen, X.Z. (2013).
780 Seismogenic structure of Lushan earthquake and its relationship with Wenchuan earthquake.
781 *Earth Science Frontiers*, 20, 11-20. (in Chinese with English abstract)

782 Xiong, S.Q. 2016. Chinese continent aeromagnetic and geological structure feature. Beijing:
783 Geological Publishing House. (in Chinese)

784 Xiong, S.Q., Fan, Z.G., Zhang, H.R., Guo, Z.H., Huang, X.Z., Ding, Y.Y., et al. (2013). Chinese
785 continent aeromagnetic map and its introduction. Beijing: Geological Publishing House, pp.
786 19. (in Chinese)

787 Yan, L. 2011. Study on the active tectonics in Longmen Mountain area and surface rupture of
788 Wenchuan earthquake. Chengdu: Chengdu university of Tecnology. (in Chinese with English
789 abstract)

790 Yan, Y.F., Teng, J.W., Ruan, X.M., & Hu, G.Z. (2016). Aeromagnetic field characteristics and the
791 Wenchuan earthquake in the Longmenshan Mountains and adjacent areas. *Chinese Journal of*
792 *Geophysical*, 59, 197-214. (in Chinese with English abstract)

793 Yi, G.X., Wen, X.Z., Xin, H., Qiao, H.Z., Wang, S.W., & Gong, Y. (2013). Stress state and
794 major-earthquake risk on the southern segment of the Longmeng Shan fault zone. *Chinese*
795 *Journal of Geophysical*, 56(4):1112-1120. (in Chinese with English abstract)

796 Yin, A., (2010). A special issue on the great 12 May 2008 Wenchuan earthquake (Mw7.9):
797 Observations and unanswered questions. *Tectonophysics*, 491, 1–9.

798 Zhan, Y., Zhao, G.Z., Unsworth, M., Wang, L.F., Chen, X.B., Li, T., et al. (2013). Deep structure
799 beneath the southwestern section of the Longmenshan fault zone and seimogenetic context of
800 the 4.20 Lushan Ms7.0 earthquake. *Chinese Sci. Bull.*, 58, 3467–3474.

801 Zhang, J.S., Gao, R., Zeng, L.S., Li, Q.S., Guan, Y., & He, R.Z., et al. (2009). Relationship

802 between characteristics of gravity and magnetic anomalies and the earthquakes in
803 Longmenshan range and adjacent areas. *Chinese Journal of Geophysics*, 52, 572-578. (in
804 Chinese with English abstract)

805 Zhang, J.S., Gao, R., Zeng, L.S., Li, Q.S., Guan, Y., & He, R.Z., et al. (2010). Relationship
806 between characteristics of gravity and magnetic anomalies and the earthquakes in the
807 Longmenshan range and adjacent areas. *Tectonophysics*, 491, 218-229.

808 Zhang, Y.Q., Teng, J.W., Wang, Q.S., & Hu, G.Z. (2014). Density structure and isostatic state of
809 the crust in the Longmenshan and adjacent areas. *Tectonophysics*, 619–620, 51–57.

810 Zhao, C.P., Zhou, L.Q., & Chen, Z.L. (2013). Source rupture process of Lushan Ms7.0 earthquake,
811 Sichuan, China and its tectonic implication. *Chin Sci Bull*, 58, 1894-1900.

812 Zhao, Y.J., Yuan, C., Zhou, M.F., Yan, D.P., Long, X.P., & Cai, K.D. (2007a). Post-orogenic
813 extension of Songpan-Ganze orogen in Early Jurassic: Constraints from Niuxingou
814 monzodiorite and Siguniangshan A-type granite of western Sichuan, China. *Geochemica*, 36,
815 139-152. (in Chinese with English abstract)

816 Zhao, Y.J., Yuan, C., Zhou, M.F., Yan, D.P., Long, X.P., & Li, J.L. (2007b). Geochemistry and
817 petrogenesis of Laojungou and Mengtonggou granites in western Sichuan, China: constraints
818 on the nature of Songpan-Ganzi basement. *Acta Perologica Sinica*, 23, 995-1006. (in Chinese
819 with English abstract)

820 Zhou, M.F., Yan, D.P., Kennedy, A.K., Li, Y.Q., & Ding J. (2002). SHRIMP U^{Pb} zircon
821 geochronological and geochemical evidence for Neoproterozoic arc-magmatism along the
822 western margin of the Yangtze Block, South China. *Earth and Planetary Science Letters*, 196,
823 51-67.

824 Zhu, Y.T., Wang, X.B., Yu, N., Gao, S.Q., Li, K., & Shi, Y.J. (2008). Deep structure of
825 magnetotelluric profile on Longmen Mts. and its relation to the Ms8.0 Wenchuan earthquake.
826 *Acta Geologica Sinica*, 82, 1769-1777. (in Chinese with English abstract)